Acta Materialia 144 (2018) 145–153

Contents lists available at ScienceDirect

Acta Materialia

journal homepage: www.elsevier.com/locate/actamat

Full length article

Strain-engineered allotrope-like bismuth nanowires for enhanced thermoelectric performance

Jeongmin Kim [a], Min-Wook Oh [b], Gwansik Kim [a], Je-Hyeong Bahk [c], Jae Yong Song [d], Seong Gi Jeon [d], Dong Won Chun [e], Jee-Hwan Bae [e], Wooyoung Shim [a, **], Wooyoung Lee [a, *]

[a] Department of Materials Science and Engineering, Yonsei University, 50 Yonsei-ro, Seodaemoon-gu, Seoul 03722, Republic of Korea
[b] Department of Advanced Materials Engineering, Hanbat National University, 125 Dongseodaero, Daejeon 305-719, Republic of Korea
[c] Department of Mechanical and Materials Engineering, University of Cincinnati, Ohio 45221, USA
[d] Materials Genome Center, Korea Research Institute of Standards and Science, Daejeon 305-340, Republic of Korea
[e] Advanced Analysis Center, Korea Institute of Science and Technology, Hwarang-ro 14-gil, Seongbuk-gu, Seoul 02792, Republic of Korea

ARTICLE INFO

Article history:
Received 12 October 2017
Accepted 27 October 2017
Available online 30 October 2017

Keywords:
Thermoelectric
Figure of merit
Strained nanowire
Bismuth nanowire
Band engineering

ABSTRACT

Allotropy is a fundamental concept that has been frequently studied since the mid-1800s. Although the bulk allotropy of elemental solids is fairly well understood, it remains challenging to reliably produce an allotrope at the nanoscale that has a different crystal structure and accompanies a change in physical properties for specific applications. Here, we demonstrate a "heterostructure" approach to produce allotrope-like bismuth nanowires, where it utilizes the lattice constant difference between bismuth and tellurium in core/shell structure. We find that the resultant strain of [100]-grown Bi nanowires increases the atomic linear density along the c-axis that has been predicted from theoretical considerations, enabling us to establish a design rule for strain-induced allotropic transformation. With our >400-nm-diameter nanowires, we measure a thermoelectric figure of merit ZT of 0.5 at room temperature with reduced thermal conductivity and enhanced Seebeck coefficient, which are primarily a result of the rough interface and the reduced band overlap according to our density-functional calculations.

1. Introduction

Allotropy is the property of atoms or molecules in more than two different structural form, but with one physical state, which exhibits different chemical and physical behaviors. Although the bulk allotropy of elemental solids is fairly well understood, it remains challenging to reliably produce an allotrope that has a different crystal structure, and thus accompanies a change in physical properties. This difficulty of producing allotropes in bulk materials also extends to the low-dimensional materials, such as nanowire, where even local strain can significantly alter nanometer-scale crystal symmetry. In the context of crystal symmetry, bismuth nanowires possess an interesting crystal anisotropy that have a highly elongated crystal structure along the c-axis, which is directly associated with its anisotropic electrical properties [1,2]. In principle, the allotropic transformation from a rhombohedral to a near-cubic structure in bismuth has been predicted to occur under a high-pressure environment, which may potentially provide the ability to control and modulate the electronic band structure [3,4]. This effect can reduce the band overlap without the size reduction that causes unwanted surface states, a reduced mean free path, and an effective mass increase [5–8]. However, the high-pressure environment for strain-induced allotropic transformation practically limits the use of the allotropic forms of bismuth. Here, we demonstrate a “heterostructure” approach that utilizes the lattice constant difference between bismuth (Bi) and tellurium (Te) in core/shell (C/S) nanowires to produce allotrope-like Bi. We find that the resultant strain of [100]-grown Bi nanowires increases the atomic linear density along the c-axis that has been predicted from theoretical considerations, enabling us to establish a design rule for strain-induced allotropic transformation. In our Bi/Te C/S nanowires, thermoelectric figure of merit *ZT* is estimated to be 0.5 at room temperature with reduced thermal conductivity κ and

* Corresponding author.
** Corresponding author.
E-mail addresses: wshim@yonsei.ac.kr (W. Shim), Wooyoung@yonsei.ac.kr (W. Lee).

https://doi.org/10.1016/j.actamat.2017.10.062
1359-6454/

enhanced Seebeck coefficient *S*, which are primarily a result of the rough interface and the reduced band overlap according to our density-functional calculations.

Owing to the highly anisotropic Fermi surface, long mean free path, and small effective mass, significant efforts have been placed on the study of unique properties of bulk Bi [1–12]. Individual nanowires have been proposed for investigating the fundamental physics as well as the potential applications of semimetal Bi using conventional nanoscale devices. Nanowire devices have been fabricated and tested to realize the potential uses of Bi using different nanowire growth means such anodic alumina templates [5,9], Ulitovsky [10], or on-film formation of nanowires (OFFON) [8,11] methods. These efforts have provided data supporting the importance of nearly defect-free high crystal quality and highly transparent electrical contacts. Because these prerequisites, which are central to studying the intrinsic behavior of charged carriers in Bi, have only been recently addressed experimentally, the realization of the unique capabilities of Bi such as thermoelectricity have been delayed [5,8–10,12].

While taking advantage of the large Bohr radius of Bi, the quantum size effects approach barely addresses the long-standing goal of creating a 'band gap', and then turns Bi into a semiconductor for potentially designing Bi-nanowire-based electronics and thermoelectrics. When the nanowire size is decreased, this limitation is hardly circumvented because of the additional surface states and the shorter mean free path [5]. Therefore, a new route for band engineering should be considered, where the size is not compromised to avoid surface state effects and to preserve a sufficient mean free path. However, few studies have succeeded in band engineering Bi nanowires without utilizing quantum size effects [13,14]. Here, we report an approach to band engineering in Bi nanowires by controlling the crystal anisotropy in the context of a lattice-mismatched heterostructure, where Te shells are incorporated onto the Bi core structures. The compressive strain associated with the different lattice constants between the Bi core and Te shell yield a reduction in the unit cell length along the trigonal axis of the Bi core (i.e., transition from rhombohedral to near-cubic structure) such that we can reduce the crystal anisotropy and thus the energy band overlap. Owing to the reduced band overlap, the thermoelectric figure of merit, *ZT*, is found to be 0.5 for the Bi/Te C/S nanowire.

2. Experimental

2.1. Sample preparations

The Bi core of Bi/Te C/S nanowires was fabricated using OFFON [11]. Bi thin films were deposited on an oxidized Si substrate using a custom-made radio-frequency (RF) sputtering system, which was evacuated to 10^{-7} Torr prior to deposition, and the vacuum was maintained during sputtering under a 2-mTorr Ar environment. The deposition of the Bi thin films was performed at 300 K with a growth rate of 44 Å/s. To grow Bi nanowires, the Bi thin films were subsequently placed in a custom-made vacuum furnace for thermal treatment. The annealing process was performed in a vacuum of 10^{-7} Torr at 250 °C for 5–10 h. The Te shell was deposited on the as-grown Bi nanowires on the substrate by RF sputtering [15]. All processes were performed in situ in a high vacuum environment to prevent oxidation.

2.2. Microstructure investigations

Structural characterization and strain analysis were performed using a transmission electron microscope (FE-TEM JEM-2100F JEOL). The Bi/Te C/S nanowires were sliced perpendicular to the growth direction by a focused ion beam (FEI Quanta 3D FEG system) for the TEM analysis.

2.3. Transport measurements

For measuring the electrical transport properties, thermoelectric devices based on an individual Bi/Te C/S nanowire were fabricated using typical electron-beam lithography (JSM-7001F JEOL and ELPHY Quantum Raith) and metallization (custom-made DC sputtering system) as shown in Fig. S1. To obtain electrical contact between the Bi core and the electrodes, the Te shell was removed using Ar plasma, followed by a Cr (5 nm)/Au (250 nm) metallization. The electrical conductivity and Seebeck coefficient were measured by nano-voltmeter (2182A KEITHLEY) and a lock-in amplifier (SR850 Stanford Research Systems), respectively. The details of the device fabrication and measurement technique have been described in Ref. [8]. For thermal conductivity measurements of nanowires, an individual Bi/Te C/S nanowire was transferred onto the two suspended membranes (silicon nitride) of the microdevice using a micro-manipulator. The two suspended membranes played a role of hot and cold junctions, respectively, which were connected by the nanowire as shown in Fig. S2. Thermal contacts between the nanowires and membranes were formed by Pt layers, which were deposited for three minutes using a FIB (FEI Quanta 3D FEG system, 2 kV/67 pA). Following the Fourier law, the thermal conductance of the nanowire was measured in a steady state of heat flow before and after removal of the nanowire. The thermal conductivity was calculated from the thermal conductance using the length and cross-sectional area of the nanowires. The detailed procedure of thermal conductivity measurement cab be found in the previous report [16,17].

2.4. DFT and BTE calculations

The band structure of Bi with strain was calculated using first-principles calculations within the density functional theorem. The anisotropic strain was applied to each c and a-axis, resembling experimental observation. We used the Vienna ab initio simulation package (VASP) [18,19] to perform total-energy calculation and structural optimization. Projector augmented-wave pseudopotentials were used [20]. The Perdew-Burke-Ernzerhof generalized gradient approximation (PBE-GGA) was employed to describe the exchange and correlation [21]. A cutoff value of 350 eV and gamma centered k-mesh of $11 \times 11 \times 11$ in the Bi primitive cell were used to ensure better than 1 meV convergence of the total energy better. Internal atomic positions were relaxed with a conjugated gradient routine in which the forces were within 0.01 eV/Å for each atom. The spin-orbit interaction (SOI) was incorporated in all calculations. The Seebeck coefficient and electrical conductivity were estimated by solving the Boltzmann transport equation (BTE) implemented in the BoltzTraP code [22] in which the rigid band approach was used. The dense k-mesh of $41 \times 41 \times 41$ was used to obtain the converged transport properties. Eigenenergies of the electronic structures without and with strain were utilized to obtain the transport properties. The relaxation time was assumed to be constant in the considered doping range. The Seebeck coefficient can be obtained without any fitting parameter from the electronic structure and BTE within the constant relaxation time approximation, whereas the calculated electrical conductivity was fitted to the experimental conductivity to estimate the value of the relaxation time. This approach proves to be good approximation (Supplementary data) [23,24].

3. Results and discussion

3.1. Allotrope-like band engineering

The anisotropic electronic band structure of Bi originates from its unique crystal structure [25]. The structure of rhombohedral Bi can be represented using a pseudo-cubic lattice by incorporating two interpenetrating face-centered cubic (FCC) sub-lattices (Fig. 1a, left panel): (i) stretch the FCC sub-lattice along one axis among the four identical diagonal axes of the FCC, (ii) overlap the FCC sub-lattices, and (iii) displace one FCC sub-lattice along the trigonal direction [25,26]. As a result, the three-fold rotational symmetry was maintained only along the direction of stretching. By convention, this stretched direction in Bi is defined as a trigonal axis (in direct lattice) and as the *T*-point of the Brillouin zone (in momentum space). On the other hand, the remaining three identical

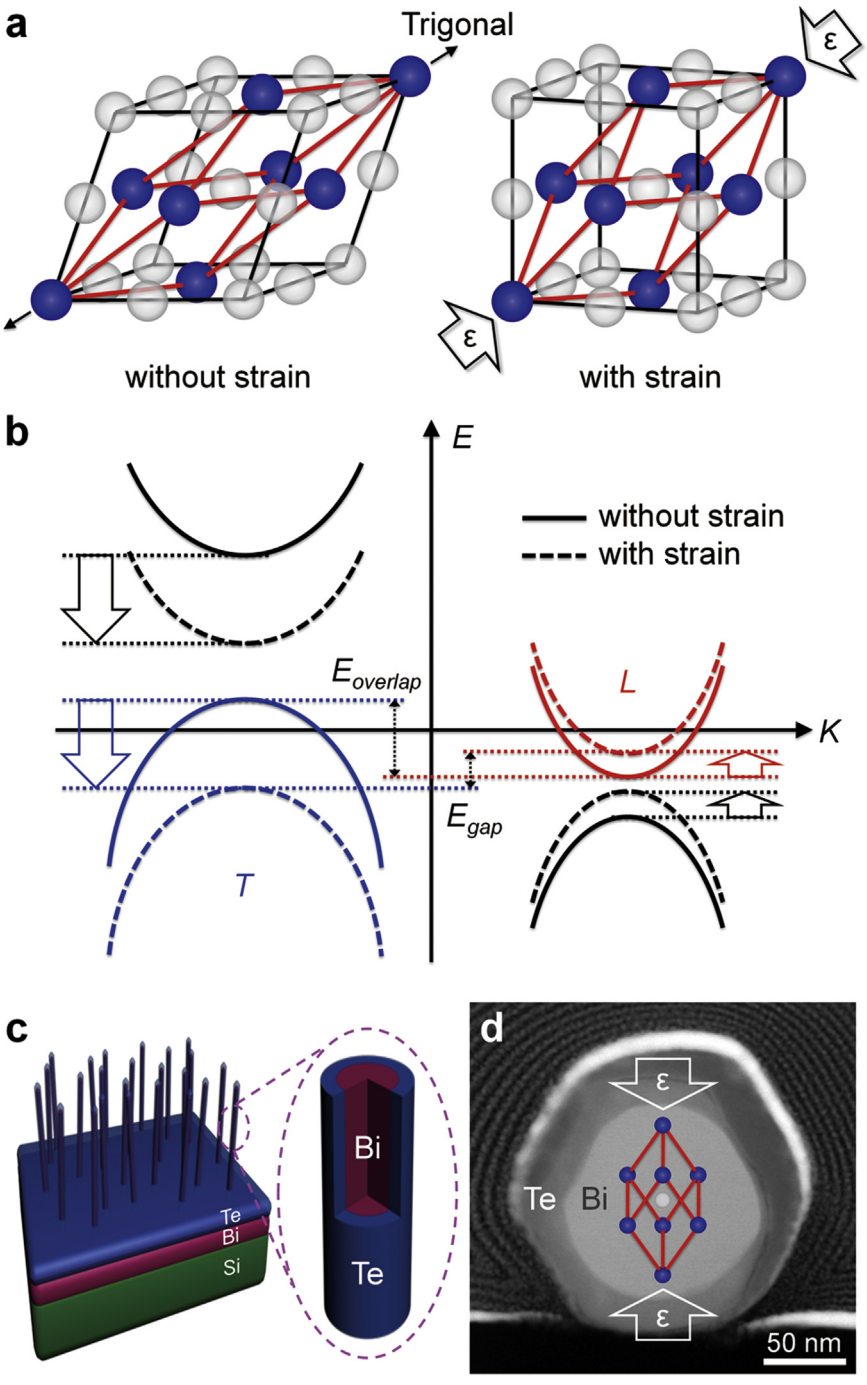

Fig. 1. Crystal and electronic band structure of the Bi core in Bi/Te C/S nanowire. a, Crystal structure of Bi with a primitive (red lines) and a pseudo-cubic (black lines) unit cell (left). Compressive strain along the trigonal axis decreases the structural anisotropy (right). In practice, the location of the second Bi atom in the primitive cell slightly migrates from the center along the trigonal axis (Fig. S3). **b**, The electronic band structure of Bi without (solid lines) and with (dashed lines) compressive strain. The compressive strain reduces the difference between the *T*- and *L*-point sub-bands as well as the structural anisotropy, resulting in a band gap opening. **c**, Schematic and **d**, low-magnification cross-sectional TEM image of the Bi/Te C/S nanowires grown by OFFON. The surrounding Te shell causes compressive strain along the trigonal axis in the Bi core. (For interpretation of the references to colour in this figure legend, the reader is referred to the web version of this article.)

diagonal axes lost the three-fold rotational symmetry as a result of stretching and are translated into *L*-points in the Brillouin zone (Fig. S3). This distortion along the trigonal axis leads to a significant variation in the electronic band structure, generating energy splitting between the *T*- and *L*-points, one hole pocket at the *T*-point, and one electron pocket at each of the three *L*-points (Fig. 1b). The semimetallic band structure of Bi, therefore, originated from the band overlap between the valence band at the *T*-point and the conduction band at the *L*-point.

We hypothesized that reduction in the lattice constant of the c-axis of Bi by compressing the trigonal axis is likely to decrease the crystal anisotropy (Fig. 1a, right panel), and decrease the band overlap by the energy splitting between *T*- and *L*-points as a result (Fig. 1b). Therefore, this strategy can induce the semimetal to semiconductor transition and is more effective than the quantum size effect because there is (1) minimal reduction in the mean free path due to the classical size effect [5], (2) less increase of carrier effective mass due to electron-hole interaction in the *L*-point subband [8], and (3) minimal surface state effects (Fig. S4) [27].

We utilize Bi/Te C/S heterostructured nanowires to compress the Bi nanowire along the trigonal axis (Fig. 1c). When the Te (a = 4.4570 and c = 5.9290 Å) shell [28] is deposited on the Bi (a = 4.5460 and c = 11.862 Å) core [29], the surface of the Bi core can be effectively strained, and there will be a strong compressive strain on the Bi core. The compressive strain associated with different lattice constants yields a reduction in the unit cell length along the trigonal axis such that we can reduce the crystal anisotropy and, thus, the energy band overlap for the Bi nanowire. Specifically, the effective compressive strain on the trigonal axis of the Bi nanowire can be realized along the growth direction of the nanowire binary axis (i.e., [100]), where the trigonal axis is normal to the area of the Te shell, as shown in Fig. 1d.

Briefly, Bi nanowires with a diameter range of 300–840 nm were grown using the OFFON method, and then a 30-nm Te shell layer was uniformly deposited on the surface of the Bi nanowire. Fig. 1d shows a representative transmission electron microscopy (TEM) image of the nanowire in which Te shell was uniformly grown on the rough surface of Bi core [15]. In this manner, we fabricated and tested the thermoelectric device elements based on single C/S nanowires, where the Bi core diameters are 300, 400, 500, 560, and 840 nm, and the Te shell thickness is 30 nm (Bi/Te C/S #1–5). To confirm the effects of the C/S heterostructure, devices based on pure Bi nanowires with diameters of 330, 470, and 500 nm were also fabricated for comparison (Pure Bi #1–3).

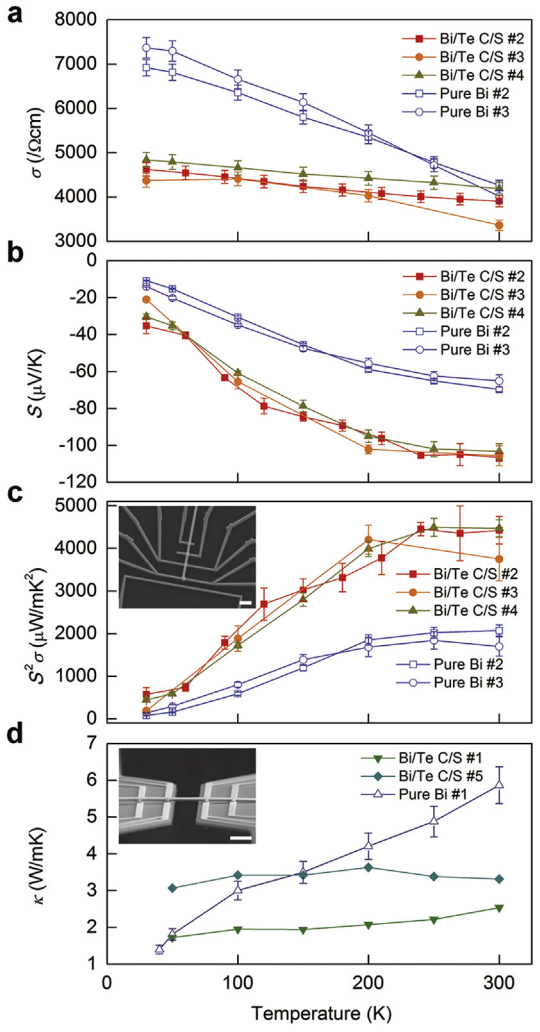

Fig. 2. Thermoelectric transport properties. a, Electrical conductivity σ, **b,** Seebeck coefficient S, **c**, power factor $S^2\sigma$, and **d,** thermal conductivity κ as a function of temperature for Bi/Te C/S and pure Bi nanowires. The insets of **c** and **d** show thermoelectric devices based on an individual nanowire for electrical (σ, S) and thermal (κ) transport properties, respectively. Scale bars represent 2 μm. The increase in the Seebeck coefficient due to the compressive strain led to an increase in the power factor despite the slight decrease in the electrical conductivity. The decrease in the thermal conductivity was caused by the strain and rough interface effects. The error bars were obtained based on the nanowire dimensions and repeated measurements.

3.2. Thermoelectric transport properties

We first investigated the effect of the strained Bi nanowires to test our hypothesis and to examine the thermoelectric properties to identify the potential applications of the Bi/Te C/S nanowires. As shown in the temperature dependence of the electrical conductivity (Fig. 2a), the Bi/Te C/S and pure Bi nanowires did not exhibit a clear dependence on the diameter in the ranges tested (namely, 460–620 nm in diameter for the Bi/Te C/S nanowires, comprising 400–560 nm for the Bi core and 30 nm for the Te shell, and 470–500 nm in diameter for the pure Bi nanowires) [8]. Therefore, the effect of the Te shell can be directly determined by comparison. The average value of the conductivity measured in the pure Bi nanowires was found to be 4140 (±176) $\Omega^{-1}\cdot cm^{-1}$ at room temperature, which was slightly smaller than that of bulk Bi (5000 Ω^{-1} cm^{-1}) due to the confined nanowire structure [9]. Note that the errors in the average values in this work include the uncertainty of the measurement such as the diameter and channel length. For the Bi/Te C/S nanowires, the average conductivity was 3820 (±420) $\Omega^{-1}\cdot cm^{-1}$ at room temperature. The reduced conductivity for the Bi/Te C/S nanowires can be explained by the low electrical conductivity of Te shell that occupies up to 20% of the cross-sectional area of the C/S nanowires (Fig. S5) [30,31]. A change in the temperature dependence was also observed. Although both the Bi/Te C/S and pure Bi nanowires exhibited metallic transport properties, the slope of conductivity as a function of temperature decreased to about one-third in the C/S nanowires (i.e., slopes of -11.29 ± 0.5 and $-2.9 \pm 0.4\ \Omega^{-1}\ cm^{-1}\ K^{-1}$ for pure Bi and Bi/Te C/S nanowires, respectively). This indicates that the influence of the carrier concentration is increased or the influence of the carrier mobility is decreased in the temperature dependence of the conductivity [8]. Although the change in the carrier concentration with temperature is significantly smaller than that of the carrier mobility in Bi, the conductivity is sensitive to the carrier concentration because of the small value of concentration [32]. Moreover, in light of the conductivity values, the carrier mobility of pure Bi and Bi/Te C/S nanowires is likely to be similar at room temperature. Therefore, the weakened metallic properties of the C/S nanowires can be

explained by a decrease in the energy band overlap in the Bi core originating from the strain effect (see below for a quantitative analysis and comparison with device experiments).

Second, as shown Fig. 2b, a dependence on diameter was not observed in the temperature-dependent Seebeck coefficient of either the Bi/Te C/S or pure Bi nanowires. The average Seebeck coefficient of a pure Bi nanowire was found to be −67.4 (±3.3) $\mu V\ K^{-1}$ in the diameter range of 470–500 nm at room temperature, which is similar to that of bulk Bi [8,33]. In the Bi/Te C/S nanowires, however, the average Seebeck coefficient was −105 (±5.4) $\mu V\ K^{-1}$ at room temperature (Fig. 2b). The enhancement of the Seebeck coefficient in the Bi/Te C/S nanowires can be explained by the semimetallic features of Bi. The negative values of the obtained Seebeck coefficient revealed that the electron contribution is dominant in the transport, but electrons and holes coexist in semimetal Bi [9]. Therefore, the Seebeck coefficient of Bi can be determined by a compromise between the electron and hole partial Seebeck coefficients of opposite signs, i.e., $S_{total} = (\sigma_e S_e + \sigma_h S_h)/(\sigma_e + \sigma_h)$, where σ is the electrical conductivity, and subscripts e and h denote electrons and holes, respectively [34]. As a result, the Seebeck coefficient of pure Bi cannot exceed several tens of $\mu V\ K^{-1}$, even though the partial Seebeck coefficients were found to be larger than several hundreds of $\mu V\ K^{-1}$, according to a theoretical study [9]. The enhancement of the Seebeck coefficient in the Bi/Te C/S nanowires can be attributed to the decrease in the hole contribution originating from the decrease in the energy band overlap caused by the strain effect (Fig. S4). Since Te possesses positive Seebeck coefficient and has very small electrical conductivity, the Te shell contribution is negligible compared to the Bi core contribution to the total Seebeck coefficient. Consequently, the power factor of the Bi/Te C/S nanowires (4216 ± 512 $\mu W\ m^{-1}\ K^{-2}$ in average) was two-fold larger than that of pure Bi nanowires (1886 ± 264 $\mu W\ m^{-1}\ K^{-2}$ in average) at room temperature, as shown in Fig. 2c, which indicates a large enhancement of the Seebeck coefficient that compromises the decrease in the electrical conductivity.

Third, the thermal conductivities of Bi/Te C/S and pure Bi nanowires were measured (Fig. 2d). Unlike the electrical conductivity and Seebeck coefficient, we observed a slight diameter dependence in the thermal conductivity of Bi/Te C/S nanowires at room temperature. In the pure Bi nanowires, the thermal conductivity has been found to exhibit a linear dependence on the diameter at room temperature, in contrast to the absence of this dependence in electrical conductivity and Seebeck coefficient at diameters greater than 200 nm [8,35]. However, the slope of the thermal conductivity as a function of diameter in the Bi/Te C/S nanowires was 20 times lower than that in the pure Bi nanowires (i.e., slopes of 1.5×10^6 and $3.2 \times 10^7\ W\ m^{-2}\ K^{-1}$ for Bi/Te C/S and pure Bi nanowires, respectively) [8]. The temperature dependence was also significantly reduced in the Bi/Te C/S nanowires. In particular, the thermal conductivities of the 360 and 900 nm Bi/Te C/S nanowires were measured to be 2.5 and 3.3 $W\ m^{-1}\ K^{-1}$, respectively, which are lower than that of the pure Bi nanowire (5.9 $W\ m^{-1}\ K^{-1}$ with a diameter of 330 nm).

The total thermal conductivity (κ_t) of semimetals consist of electronic (κ_e) and lattice (κ_l) components [36]. The electronic thermal conductivity can be estimated by means of electrical conductivity using the Wiedemann-Franz law, $\kappa_e = L\sigma T$, where L is the Lorenz number [37]. Therefore, the thermal conductivities of Bi/Te C/S nanowires at the diameters and temperatures where the electrical conductivity was measured were interpolated from the measured thermal conductivity according to the obtained diameter dependence (Fig. 3a). Because the thermal conductivity shows very small dependence on diameter, the error in the interpolation is expected to be sufficiently small relative to the interpolated values. However, in order to confirm that the errors caused by the interpolation do not cause appreciable changes in the final results such as the lattice thermal conductivity and thermoelectric figure of merit, we arbitrarily set a large error corresponding to the difference between the two boundaries (κ for 360 and 900 nm). Usually, the Lorenz number used to obtain the electronic thermal conductivity ranges from $1.49 \times 10^{-8}\ W\ \Omega\ K^{-2}$ for non-degenerated semiconductors to $2.44 \times 10^{-8}\ W\ \Omega\ K^{-2}$ for metals and strongly degenerated semiconductors [37–39]. Since the Bi/Te C/S nanowires consist of a semimetal and non-degenerated semiconductor, the Lorenz number is expected to be between these two limiting values. We calculated the Lorenz number based on the reduced Fermi energy obtained from the Seebeck coefficient, as shown in Fig. 3b (Fig. S6). The Lorenz number of the Bi/Te C/S nanowires was found to be about $1.9 \times 10^{-8}\ W\ \Omega\ K^{-2}$ at room temperature, which is in good agreement with the values reported in previous studies on nanowires based on semiconductors and metals [40–43]. Moreover, a study on the transverse thermomagnetic effect on thermal conductivity revealed that the Lorenz number of Bi is smaller than the Sommerfeld value ($2.44 \times 10^{-8}\ W\ \Omega\ K^{-2}$), even when the electronic thermal conductivity contained a bipolar contribution [36]. Moreover, in semimetals and semiconductors, wherein electrons and holes coexist, the bipolar contribution can be appreciable when both the carrier mobility and concentration of electrons and holes are equal [38]. The mobility of holes in Bi is about 10 times smaller than that of electrons [44]. Furthermore, the reduction in the energy band overlap caused by strain leads to a decrease in the hole contribution to transport, as evident by the enhanced contribution of electrons to the Seebeck coefficient in the Bi/Te C/S nanowires. Therefore, in our Bi/Te C/S heterostructure, the bipolar contribution to the electronic thermal conductivity may be unappreciable. Recent reports have shown that nano- and heterostructuring can also lead to a reduction in the bipolar contribution [45–48]. As shown in Fig. 3c and d, the electronic and lattice thermal conductivities of the Bi/Te C/S nanowires were estimated using the relation $\kappa_l = \kappa_t - \kappa_e$. Together, these graphs suggest that the decrease in the thermal conductivity of the C/S nanowires at room temperature is dominated by the suppression of the lattice thermal conductivity. There are several factors contributing to thermal conductivity reduction in C/S structure. Firstly, we have explicitly investigated the effect of strain (−2.5%, that is comparable to the strain induced in C/S nanowire in this study) in a bulk single crystal Bi, where the interface effect is not considered. The values of thermal conductivity reduction for binary and trigonal directions were 8 and 10%, respectively. The decrease in thermal conductivity with compressive strain along trigonal direction is expected given that the frequency-specific phonons propagating in the Bi atoms undergo more scattering (Fig. S7). The observed reduction could be further compensated for by adopting the interface effect, although even without such consideration the reduction remains sufficiently large to enhance the thermoelectric figure of merit. The presence of interface in C/S nanowire is important such that the roughness can reduce phonon mean free path by phonon scattering [49], and the phonon-mode interference at the interface can suppress phonon modes in carrying out the heat conduction in C/S structures [50–52]. The combined effect at the interface allows thermal conductivity to be lowered by 80% compared to pure Bi nanowires at a diameter above 300 nm [15]. Indeed, the molecular dynamic studies on Si/Ge C/S nanowires revealed that the heterogeneous interface leads to not only the significant localization of long-wavelength phonon modes, but also the depression of high frequency non-propagating phonon modes in whole body of the C/S structure [50,51]. These theoretical studies have predicted the significant reduction in thermal conductivity by up to 88%, which

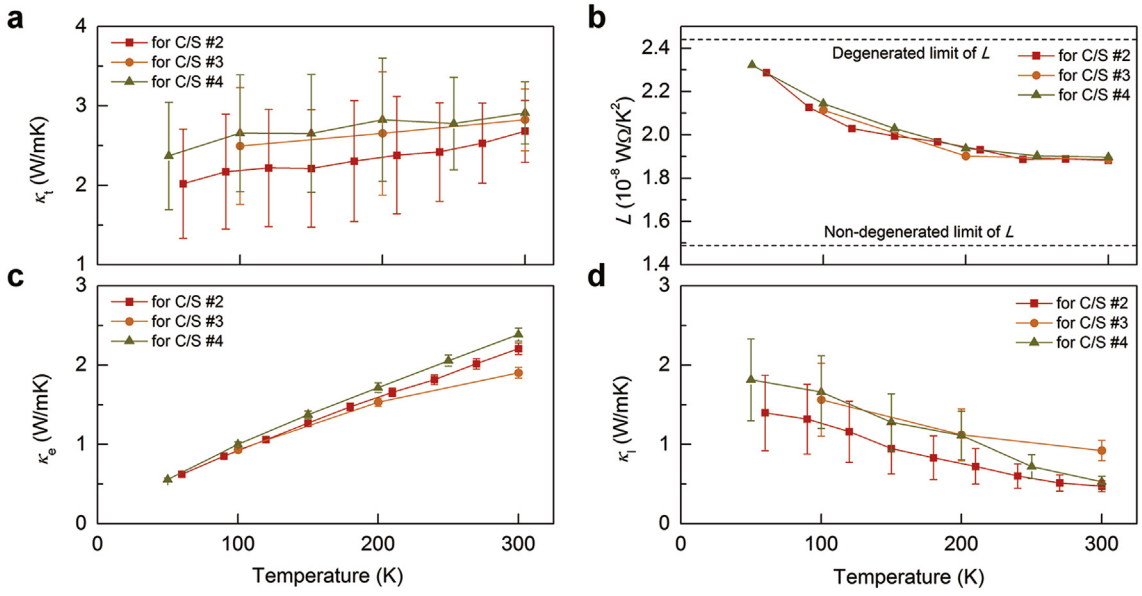

Fig. 3. Calculation of the thermal transport properties. a, Total thermal conductivity κ_t interpolated from the measured data, **b,** Lorenz number L calculated using the reduced Fermi energy of Bi/Te C/S nanowires as a function of temperature, **c,** electronic thermal conductivity κ_e, and **d,** lattice thermal conductivity κ_l estimated using the obtained Lorenz number, indicating that the decrease in the thermal conductivity of the C/S nanowires originated from the suppression of the lattice contribution at room temperature. The error in the interpolation was assumed to be the difference between the upper and lower limits of the measured data.

was demonstrated experimentally with considerable depression of phonon modes in Si/Ge C/S nanowires [52]. In addition, we note that low temperature and diameter dependences of thermal conductivity in Bi/Te C/S nanowires, compared to the pure Bi nanowire, imply that the depression of phonon modes can also lead to decrease of thermal conductivity [50,52].

Finally, we investigated the thermoelectric figure of merit, $ZT = \sigma S^2 T/\kappa$, of the Bi/Te C/S nanowires compared to the pure Bi nanowires as shown in Fig. 4. To estimate ZT, we used power factors of Bi/Te C/S #2–4 and of pure Bi #2 and 3 and the thermal conductivities interpolated from the measured data of Bi/Te C/S #1 and 5 and of Bi #1. The obtained ZT in the Bi/Te C/S nanowire is about 0.5, which is approximately seven times larger than that of a pure Bi nanowire ($ZT = 0.07$). The enhanced ZT can be explained with (1) the doubled power factor owing to the reduction in energy band overlap (see following quantitative analysis) and (2) reduction of thermal conductivity due to the suppression of the phonon mode and transport in the strained Bi core and the rough interface between the Bi core and Te shell.

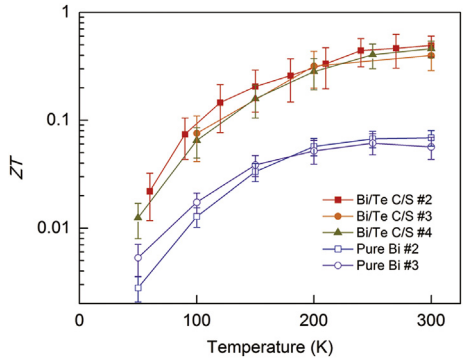

Fig. 4. Thermoelectric figure of merit. Dimensionless figure of merit ZT as a function of temperature for Bi/Te C/S and pure Bi nanowires. The dimensionless figure of merit of Bi/Te C/S nanowires is greater than that of pure Bi nanowires, which could be attributed to the strain and interface effects induced by the Te shell.

3.3. TEM and strain analysis

Next, to validate our hypothesis, we have conducted TEM investigations for a Bi/Te C/S nanowire of $d = 460$ nm to show the presence of compressive strain in the Bi core (Fig. 5a). The high-resolution TEM (HRTEM) images and lattice-fringe spacings of the Bi/Te C/S nanowire were obtained at distance intervals of 50 nm from the C/S interface (Fig. 5a(I)–(V)), and a pure Bi nanowire was also measured for reference (Fig. 5a(Bi NW)). The lattice-fringe spacings was obtained by the fast Fourier transform (FFT) in each HRTEM image. The growth direction of two different Bi nanowires was found to be along the binary axis, which is perpendicular to the trigonal axis (Fig. S8). From the lattice-fringe spacing measurements of the (003) and (0–11) planes, the lattice constants in the hexagonal lattice system were calculated. For the pure Bi nanowire, the lattice constants were found to be a = 4.547 and c = 11.865 Å, which are nearly identical with that of bulk Bi (a = 4.546 and c = 11.862 Å) [29]. For the Bi/Te C/S nanowire, on the other hand, the lattice constants were calculated to be smaller than those of the pure Bi nanowire. For example, the lattice constant of the a-axis for regions I, II, III, IV, and V (indicated in Fig. 5a(I)–(V)) are 4.532, 4.519, 4.526, 4.518, and 4.520 Å, respectively. In particular, there was a significant reduction of the lattice constant along the c-axis compared to the a-axis. The measured lattice constants of c-axis for regions I, II, III, IV, and V are 11.496, 11.592, 11.646, 11.670, and 11.730 Å, respectively. Based on the HRTEM analysis, the measured strain of the a- and c-axis as a function of the distance from interface of C/S is shown in Fig. 5b. Importantly, the compressive strain along the c-axis was significantly larger than that along a-axis. Moreover, the compressive strain along the c-axis decreased with increasing distance from the interface, indicating that the Te shell is the origin of the strain. Furthermore, defects and dislocations were found in Te shell with a tensile strain, while the Bi core is highly single-crystalline with the compressive strain (Fig. S9). The average strain along c-axis in the Bi core could be calculated at −2.5% according to the cross-sectional distribution of strain (Fig. 5b inset). These findings show that Bi/Te C/S structures provide

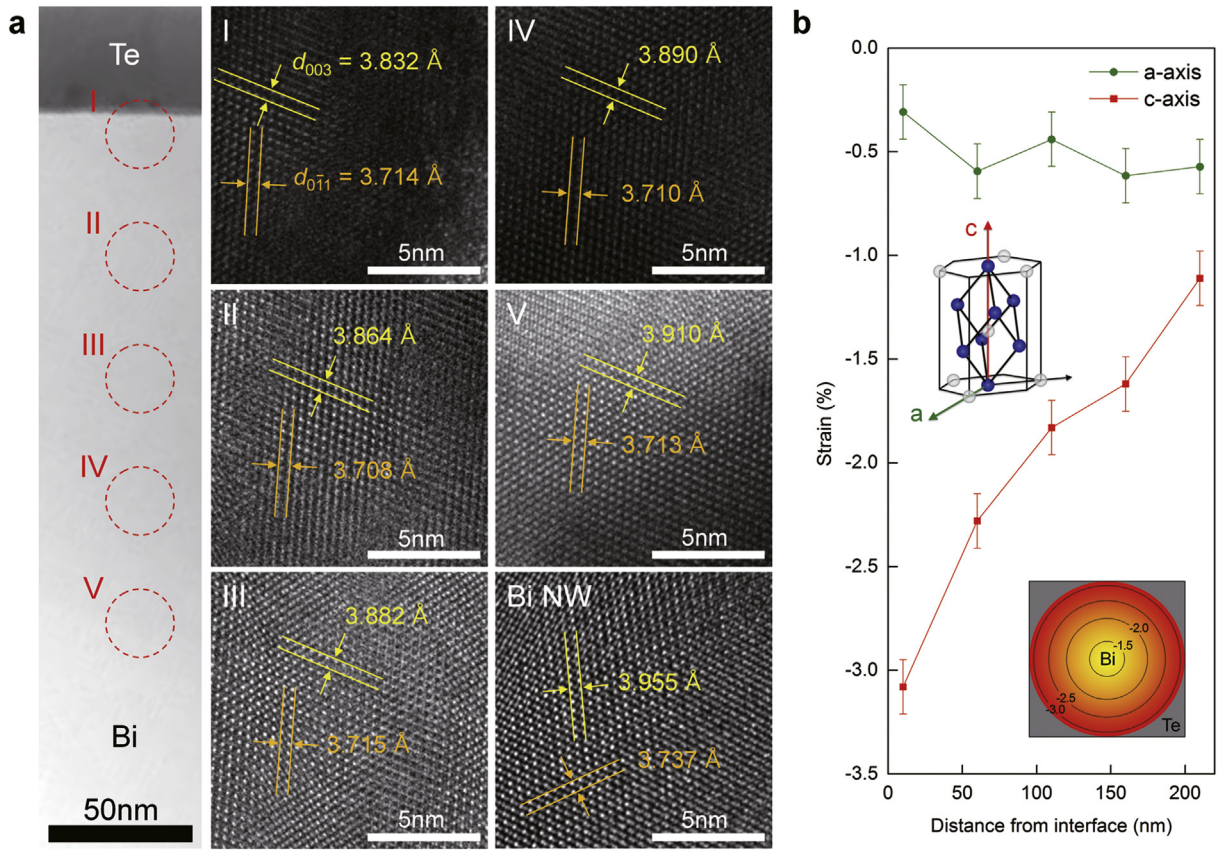

Fig. 5. TEM and strain analysis. a, Low-magnification and high-resolution TEM images of a Bi/Te C/S nanowire with a diameter of 460 nm. The lattice-fringe of the (003) plane decreased near the interface. **b**, Strain in the Bi core along the a- and c-axis as a function of the distance from the interface. The a- and c-axis in the hexagonal lattice system of Bi (upper inset) are identical to the binary and trigonal axis in the Cartesian coordination system, respectively. The bottom inset represents the cross-sectional distribution of strain in the Bi core.

a route for generating strain that alters the crystal structure. Together with surface morphology control for the suppression of thermal conductance [49], depositing a Te shell on Bi core is a distinct technique from previous studies in that it simultaneously meets requirements of thermoelectric applications: low thermal conductivity and high power factor.

3.4. Theoretical analysis

Last, we have performed a theoretical analysis of the band structure with and without strain: (1) the band structures were obtained using first-principles calculations within the density functional theory (DFT) (Fig. 6a and b), and (2) the Seebeck coefficient and electrical conductivity were estimated by solving the Boltzmann transport equation (Fig. 6c). First, without the strain, the first-principles calculation shows the semimetallic nature of Bi, where the Fermi level was degenerate with a hole sub-band at the *T*-point and an electron sub-band at the *L*-point (Fig. 4a, left panel). The calculated band overlap in this study was 162 meV, which is good agreement with the previously calculated value (163 meV) using DFT [53]. However, the band overlap energy obtained using DFT could be overestimated; the calculated values are much larger than that of the reported value (98 meV) in Bi [54]. Nonetheless, a strong agreement between the experiment (Fig. 2a) and calculation (Fig. 6a, left panel) demonstrate that unstrained Bi exhibits metallic behavior with band overlap. Second, with the strain of −2.5% (i.e., compressive strain) along the c-axis, there was a position change of the sub-bands at the *T*- and *L*-point (Fig. 6a, right panel): the overlap energy between the valence band at the *T*-point and conduction band at the *L*-point is reduced to 80 meV (Fig. 6b). In this sense, the low anisotropy in Bi with the strain modeled in Fig. 1b can be validated by the decrease of *T*- and increase of *L*-point sub-bands in that (1) pair-sub-bands (i.e., pair of the conduction and valence bands at each point in momentum space) shifted toward a similar energy level, and (2) the band gap energy of each pair-sub-band became comparable (Fig. 6b inset). According to the calculation, the compressive strain along the a-axis, leading to higher anisotropy, causes the increase of *T*- and decrease of *L*-point sub-bands and thus increases the band overlap. Given that the band overlap is ultimately governed by crystal anisotropy, further reduction in the band overlap by tensile strain along the a-axis is possible (Fig. S10).

Finally, the Seebeck coefficient and the electrical conductivity of Bi without and with strain were estimated from electronic the band structure and the Boltzmann transport equation (Fig. 6c). Note that the Seebeck coefficient can be directly obtained from the band structure if the relaxation time is constant. Thus, we compared the experimental value of the Seebeck coefficient with the calculated value without any fitting parameter. For the system without strain, the experimental value of −69.7 μV K^{-1} could be obtained at 3.7 × 10^{19} cm^{-3}. This large carrier concentration originated from the overestimation of the band overlap energy and it could be corrected to 6.7 × 10^{18} cm^{-3} for the overlap energy of 98 meV. Note that from the calculations of the system without strain, we could

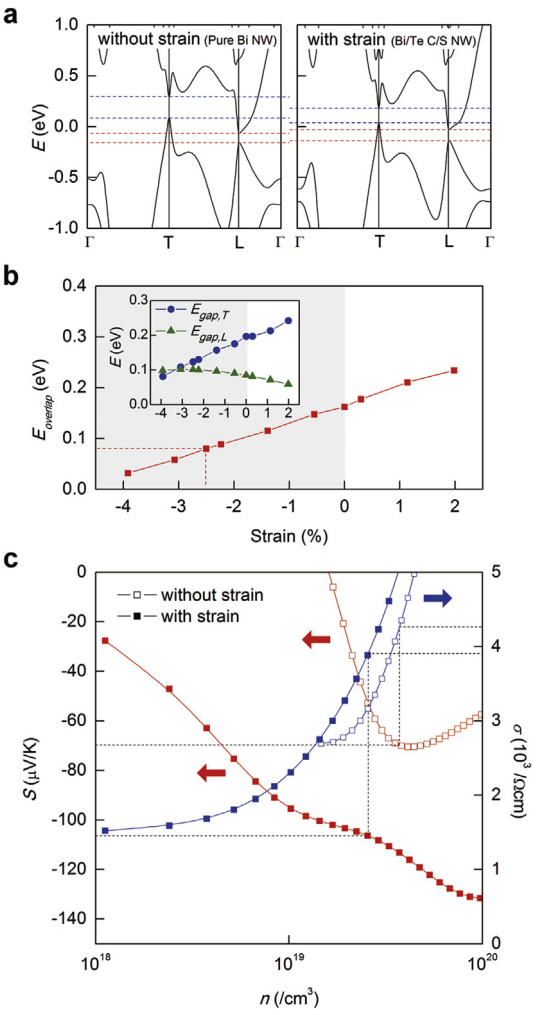

Fig. 6. Theoretical band structure and thermoelectric transport properties. a, Electronic band structure of Bi without and with strain (−2.5%) along the c-axis obtained by first-principles calculation. The compressive strain reduced the anisotropy of the band structure, resulting in a decrease of the band overlap energy. **b**, Band overlap energy of Bi as a function of strain. Inset shows the variation of the band gap energy of each sub-band at the *T*- and *L*-point. However, the band overlap energy obtained using first-principles calculations could be overestimated.[43] **c**, Seebeck coefficient (red) and electrical conductivity (blue) as a function of the carrier concentration, estimated from the band structures without (open squares) and with (solid squares) strain. The measured values without and with strain were consistent with calculated values at 3.7×10^{19} and 2.8×10^{19} cm^{-3}, respectively. The carrier concentrations, which were larger than those of the experimentally achieved for the corresponding Seebeck coefficient, originated from the overestimation of the band overlap energy. (For interpretation of the references to colour in this figure legend, the reader is referred to the web version of this article.)

not obtain such a large experimentally observed value of -106.4 μV K^{-1} in Bi/Te C/S nanowire. For the system with strain, however, the experimental value (-106.4 μV K^{-1}) could be obtained at 2.6×10^{19} cm^{-3}. The corresponding carrier concentration is thought to be overestimated due to overestimation of the overlap energy. To estimate the electrical conductivity, the relaxation time was needed. The relaxation times for the systems without and with strain were estimated as 4.9×10^{-14} s and 1.6×10^{-14} s, respectively, by fitting the calculated values at the above-mentioned carrier concentrations with the experimental values. The reduced relaxation time suggests that electrons are more scattered in the strained system, which could be attributed to the change in the deformation potential scattering due to the compressive strain.

4. Conclusion

Our studies demonstrate that lattice-mismatched heterostructures consisting of a Te shell and Bi core nanowire reduce the crystal anisotropy of the Bi core. The reduced anisotropy can further reduce the band overlap in the Bi core, thus providing a new approach for realizing band engineering for thermoelectric applications. Compared to the quantum size effects, this approach represents a new synthetic heterostructured nanowire with several unique advantages, including (1) a larger nanowire diameter that does not suppress the electrical mean free path, (2) a low surface-to-volume ratio where the surface state does not considerably matter, and (3) an apparent *T*-point band shift preventing an increase of the electron effective mass. The functionality of the C/S nanowire for thermoelectric application was demonstrated with enhanced power factor and reduced thermal conductivity, leading to *ZT* of 0.5 at room temperature. This level of thermoelectric efficiency is substantially greater than pure Bi nanowires ($ZT = 0.07$) and bulk Bi ($ZT < 0.05$). We believe that the Bi/Te C/S nanowires constitute a new family of materials capable of crystallographic alteration, which will extend the scope of fundamental and applied materials science for identifying potential allotropy.

Acknowledgments

This work was supported by the National Research Foundation of Korea (NRF) grant funded by the Korea government (MSIT) (2017R1A2A1A17069528).

Appendix A. Supplementary data

Supplementary data related to this article can be found at https://doi.org/10.1016/j.actamat.2017.10.062.

References

[1] F.Y. Yang, K. Liu, K.M. Hong, D.H. Reich, P.C. Searson, C.L. Chien, Large magnetoresistance of electrodeposited single-crystal bismuth thin films, Science 284 (5418) (1999) 1335–1337.
[2] T.W. Cornelius, M.E.T. Molares, Nanowires, InTech, Shanghai, 2010.
[3] J.R. Vaišnys, R.S. Kirk, Effect of pressure on the electrical properties of bismuth, J. Appl. Phys. 38 (11) (1967) 4335–4337.
[4] N.P. Armitage, R. Tediosi, F. Lévy, E. Giannini, L. Forro, D. van der Marel, Infrared conductivity of elemental bismuth under pressure: evidence for an avoided lifshitz-type semimetal-semiconductor transition, Phys. Rev. Lett. 104 (23) (2010) 237401.
[5] T.E. Huber, A. Adeyeye, A. Nikolaeva, L. Konopko, R.C. Johnson, M.J. Graf, Surface state band mobility and thermopower in semiconducting bismuth nanowires, Phys. Rev. B Condens. Matter Mater. Phys. 83 (23) (2011) 235414.
[6] J. Kim, S. Lee, Y.M. Brovman, M. Kim, P. Kim, W. Lee, Weak antilocalization and conductance fluctuation in a single crystalline Bi nanowire, Appl. Phys. Lett. 104 (4) (2014) 043105.
[7] J. Kim, D. Kim, T. Chang, W. Lee, Quantum size effect on Shubnikov-de Haas oscillations in 100 nm diameter single-crystalline bismuth nanowire, Appl. Phys. Lett. 105 (12) (2014) 123107.
[8] J. Kim, S. Lee, Y.M. Brovman, P. Kim, W. Lee, Diameter-dependent thermoelectric figure of merit in single-crystalline Bi nanowires, Nanoscale 7 (2015) 5053–5059.
[9] J. Heremans, C.M. Thrush, Thermoelectric power of bismuth nanowires, Phys. Rev. B Condens. Matter Mater. Phys. 59 (19) (1999) 12579–12583.
[10] A. Nikolaeva, T.E. Huber, D. Gitsu, L. Konopko, Diameter-dependent thermopower of bismuth nanowires, Phys. Rev. B Condens. Matter Mater. Phys. 77 (3) (2008) 035422.
[11] W. Shim, J. Ham, K.I. Lee, W.Y. Jeung, M. Johnson, W. Lee, On-film formation of Bi nanowires with extraordinary electron mobility, Nano Lett. 9 (1) (2009) 18–22.
[12] J. Kim, W. Shim, W. Lee, Bismuth nanowire thermoelectrics, J. Mater. Chem. C 3 (46) (2015) 11999–12013.
[13] O. Rabin, Y.M. Lin, M.S. Dresselhaus, Anomalously high thermoelectric figure of merit in Bi1-x-Sbx nanowires by carrier pocket alignment, Appl. Phys. Lett. 79 (1) (2001) 81–83.
[14] Y.-M. Lin, O. Rabin, S.B. Cronin, J.Y. Ying, M.S. Dresselhaus, Semimetal–semiconductor transition in Bi1−xSbx alloy nanowires and their thermoelectric properties, Appl. Phys. Lett. 81 (13) (2002) 2403–2405.

[15] J. Kang, J.W. Roh, W. Shim, J. Ham, J.-S. Noh, W. Lee, Reduction of lattice thermal conductivity in single Bi-Te core/shell nanowires with rough interface, Adv. Mater 23 (30) (2011) 3414–3419.
[16] H.S. Shin, S.G. Jeon, J. Yu, Y.-S. Kim, H.M. Park, J.Y. Song, Twin-driven thermoelectric figure-of-merit enhancement of Bi2Te3 nanowires, Nanoscale 6 (11) (2014) 6158–6165.
[17] S.G. Jeon, D.W. Park, H.S. Shin, H.M. Park, S.Y. Choi, S.J. Lee, J. Yu, J.Y. Song, Effects of doping and planar defects on the thermoelectric properties of InAs nanowires, RSC Adv. 6 (10) (2016) 7791–7797.
[18] G. Kresse, J. Hafner, *Ab initio* molecular dynamics for liquid metals, Phys. Rev. B Condens. Matter Mater. Phys. 47 (1) (1993) 558–561.
[19] G. Kresse, J. Hafner, *Ab initio* molecular-dynamics simulation of the liquid-metal–amorphous-semiconductor transition in germanium, Phys. Rev. B Condens. Matter Mater. Phys. 49 (20) (1994) 14251–14269.
[20] P.E. Blöchl, Projector augmented-wave method, Phys. Rev. B Condens. Matter Mater. Phys. 50 (24) (1994) 17953–17979.
[21] J.P. Perdew, K. Burke, M. Ernzerhof, Generalized gradient approximation made simple, Phys. Rev. Lett. 77 (18) (1996) 3865–3868.
[22] G.K.H. Madsen, D.J. Singh, BoltzTraP. A code for calculating band-structure dependent quantities, Comput. Phys. Commun. 175 (1) (2006) 67–71.
[23] M.W. Oh, D.M. Wee, S.D. Park, B.S. Kim, H.W. Lee, Electronic structure and thermoelectric transport properties of AgTlTe: first-principles calculations, Phys. Rev. B Condens. Matter Mater. Phys. 77 (16) (2008) 165119.
[24] J.Y. Kim, M.-W. Oh, S. Lee, Y.C. Cho, J.-H. Yoon, G.W. Lee, C.-R. Cho, C.H. Park, S.-Y. Jeong, Abnormal drop in electrical resistivity with impurity doping of single-crystal Ag, Sci. Rep. 4 (2014) 5450.
[25] P. Hofmann, The surfaces of bismuth: structural and electronic properties, Prog. Surf. Sci. 81 (5) (2006) 191–245.
[26] O. Rabin, Bismuth Nanowire and Antidot Array Studies Motivated by Thermoelectricity, , Department of Chemistry, Massachusetts Institute of Technology, Cambridge, 2004.
[27] A. Nikolaeva, D. Gitsu, L. Konopko, M.J. Graf, T.E. Huber, Quantum interference of surface states in bismuth nanowires probed by the Aharonov-Bohm oscillatory behavior of the magnetoresistance, Phys. Rev. B Condens. Matter Mater. Phys. 77 (7) (2008) 075332.
[28] W.M. Haynes, CRC Handbook of Chemistry and Physics, CRC Press, 2012.
[29] C.S.B.D. Schiferl, The crystal structure of arsenic at 4.2, 78 and 299 K, J. Appl. Crystallo. 2 (1) (1969) 30–36.
[30] A. Nussbaum, Electrical properties of pure tellurium and tellurium-selenium alloys, Phys. Rev. 94 (2) (1954) 337–342.
[31] V.E. Bottom, The hall effect and electrical resistivity of tellurium, Science 115 (2995) (1952) 570–571.
[32] Z.B. Zhang, X.Z. Sun, M.S. Dresselhaus, J.Y. Ying, J. Heremans, Electronic transport properties of single-crystal bismuth nanowire arrays, Phys. Rev. B Condens. Matter Mater. Phys. 61 (7) (2000) 4850–4861.
[33] B.S. Chandrasekhar, The seebeck coefficient of bismuth single crystals, J. Phys. Chem. Solids 11 (3–4) (1959) 268–273.
[34] L.D. Hicks, M.S. Dresselhaus, Effect of quantum-well structures on the thermoelectric figure of merit, Phys. Rev. B Condens. Matter Mater. Phys. 47 (19) (1993) 12727–12731.
[35] J.W. Roh, K. Hippalgaonkar, J.H. Ham, R.K. Chen, M.Z. Li, P. Ercius, A. Majumdar, W. Kim, W. Lee, Observation of anisotropy in thermal conductivity of individual single-crystalline bismuth nanowires, Acs Nano 5 (5) (2011) 3954–3960.
[36] C. Uher, H.J. Goldsmid, Separation of the electronic and lattice thermal conductivities in bismuth crystals, Phys. Status Solidi B 65 (2) (1974) 765–772.
[37] V.I. Fistul, Heavily Doped Semiconductors, Plenum Press, New York, 1969.
[38] T.M. Tritt, Thermal Conductivity, Kluwer Academic/Plenum Publisher, New York, 2004.
[39] L. Zhou, P. Qiu, C. Uher, X. Shi, L. Chen, Thermoelectric properties of p-type YbxLayFe2.7Co1.3Sb12 double-filled skutterudites, Intermetallics 32 (2013) 209–213.
[40] E.Z. Xu, Z. Li, J.A. Martinez, N. Sinitsyn, H. Htoon, N. Li, B. Swartzentruber, J.A. Hollingsworth, J. Wang, S.X. Zhang, Diameter dependent thermoelectric properties of individual SnTe nanowires, Nanoscale 7 (7) (2015) 2869–2876.
[41] F. Völklein, H. Reith, T.W. Cornelius, M. Rauber, R. Neumann, The experimental investigation of thermal conductivity and the Wiedemann–Franz law for single metallic nanowires, Nanotechnology 20 (32) (2009) 325706.
[42] F. Völklein, H. Reith, M.C. Schmitt, M. Huth, M. Rauber, R. Neumann, Microchips for the investigation of thermal and electrical properties of individual nanowires, J. Electron. Mater 39 (9) (2010) 1950–1956.
[43] C.-H. Chien, P.-C. Lee, W.-H. Tsai, C.-H. Lin, C.-H. Lee, Y.-Y. Chen, In-situ observation of size and irradiation effects on thermoelectric properties of Bi-Sb-Te nanowire in FIB trimming, Sci. Rep 6 (2016) 23672.
[44] D.L. Partin, J. Heremans, D.T. Morelli, C.M. Thrush, C.H. Olk, T.A. Perry, Growth and characterization of epitaxial bismuth films, Phys. Rev. B Condens. Matter Mater. Phys. 38 (6) (1988) 3818–3824.
[45] B. Poudel, Q. Hao, Y. Ma, Y. Lan, A. Minnich, B. Yu, X. Yan, D. Wang, A. Muto, D. Vashaee, X. Chen, J. Liu, M.S. Dresselhaus, G. Chen, Z. Ren, High-thermoelectric performance of nanostructured bismuth antimony telluride bulk alloys, Science 320 (5876) (2008) 634–638.
[46] W. Xie, J. He, H.J. Kang, X. Tang, S. Zhu, M. Laver, S. Wang, J.R.D. Copley, C.M. Brown, Q. Zhang, T.M. Tritt, Identifying the specific nanostructures responsible for the high thermoelectric performance of (Bi,Sb)2Te3 nanocomposites, Nano Lett. 10 (9) (2010) 3283–3289.
[47] J.-H. Bahk, A. Shakouri, Enhancing the thermoelectric figure of merit through the reduction of bipolar thermal conductivity with heterostructure barriers, Appl. Phys. Lett. 105 (5) (2014) 052106.
[48] S. Wang, J. Yang, T. Toll, J. Yang, W. Zhang, X. Tang, Conductivity-limiting bipolar thermal conductivity in semiconductors, Sci. Rep. 5 (2015) 10136.
[49] A.I. Hochbaum, R. Chen, R.D. Delgado, W. Liang, E.C. Garnett, M. Najarian, A. Majumdar, P. Yang, Enhanced thermoelectric performance of rough silicon nanowires, Nature 451 (7175) (2008) 163–167.
[50] M. Hu, X. Zhang, K.P. Giapis, D. Poulikakos, Thermal conductivity reduction in core-shell nanowires, Phys. Rev. B Condens. Matter Mater. Phys. 84 (8) (2011) 085442.
[51] M. Hu, K.P. Giapis, J.V. Goicochea, X. Zhang, D. Poulikakos, Significant reduction of thermal conductivity in Si/Ge Core–Shell nanowires, Nano Lett. 11 (2) (2011) 618–623.
[52] T.-K. Hsiao, B.-W. Huang, H.-K. Chang, S.-C. Liou, M.-W. Chu, S.-C. Lee, C.-W. Chang, Micron-scale ballistic thermal conduction and suppressed thermal conductivity in heterogeneously interfaced nanowires, Phys. Rev. B Condens. Matter Mater. Phys. 91 (3) (2015) 035406.
[53] A.B. Shick, J.B. Ketterson, D.L. Novikov, A.J. Freeman, Electronic structure, phase stability, and semimetal-semiconductor transitions in Bi, Phys. Rev. B Condens. Matter Mater. Phys. 60 (23) (1999) 15484–15487.
[54] A.J. Levin, M.R. Black, M.S. Dresselhaus, Indirect L to T point optical transition in bismuth nanowires, Phys. Rev. B Condens. Matter Mater. Phys. 79 (16) (2009) 165117.